

# A Transient Based Phase Selection Method for Transmission Line Protection

M. N. Haleem, A. D. Rajapakse

**Abstract**— A comprehensive and fast faulty phase selection method based on local current transients is presented in this paper. Faulty phase selection in transient based protection relays is considered to be very challenging as it requires making decisions within sub-cycle time period and while transients are dependent on many parameters such as fault resistance and fault inception angle. Three indices are defined for each combination of phase currents. Each index compares the magnitudes of the rate of change of current through two associated phases. A systematic logic is introduced to identify different types of faults and the faulted phases. As the proposed indices do not vary with the fault resistance, faulty phase selection can be reduced to a manageable problem that can be handled with threshold-based comparison and it can be easily implemented on low-cost hardware. Very accurate predictions are observed during the rigorous evaluation carried at different fault locations and for different fault inception angles and resistances.

**Keywords:** Phase selection, transient based protection, fault classification.

## I. INTRODUCTION

TRANSIENT-BASED protection techniques offer certain advantages over the traditional fundamental frequency phasor based protection algorithms, and are being actively investigated [1]. Types of decisions made in a transient based protection relay includes detecting the presence of a fault, identifying the phases involved in the fault, and making sure that the fault is within the protected zone. Identifying phases involved in the fault, often-called phase selection, is a challenging task as it has to be completed within the sub-cycle period during which the fault transients exist. A fault generated transient signal is influenced by many factors such as the fault inception angle, fault resistance, and the location of fault in addition to the fault type itself [2]. If traditional power frequency based phase selection algorithms are employed with transient based fault detection and discrimination schemes, the speed advantage of transient based protection will be lost [3]. Therefore, high frequency fault generated transients that contains information of fault type among others, is often used in fault classification as proposed in [1] - [4]. Rapid development of hardware such as high speed digital signal processing (DSP) chips and high speed microprocessor chips makes it possible to implement such algorithms at low cost [1].

Wavelet transform (WT) is a tool that is often used to

capture the high-frequency traveling waves for fault detection, classification, and phase selection [4], and examples can be found in [1]. The fault-induced transients can be overdamped for specific fault inception angles during single line-to-ground (SLG) and line-to-tine (LL) faults. However, several methods are claimed for accurate detection of fault-induced transients for any fault inception angle even with this limitation [5]. Transient based fault detection schemes even applied for single line-to-ground fault detection, such as [6], can be found literature. Due to challenging nature of complex feature extraction and classification, WT based systems are often used with tools like artificial neural networks (ANN) [1,2], or fuzzy logic [7] in fault classification. Design of systems with customized fault classifiers using such techniques is a very complicated task as they demand large sets of training data and time consuming training [4].

A comprehensive and fast approach of classifying the fault type and identifying the faulty phases based on the initial part of fault generated current transient is presented in this paper. The method can be implemented with transient based distance protection schemes such as [8]. Three indices are defined considering different combinations of two phase currents. Each of these indices reflects relative magnitudes of the rate of change of current through the two phases considered. The proposed method has many advantages. It relies only on current measurements and avoids the need of specially designed transducers for voltage measurements, as traditional CVTs distort the transients [9]. The calculated indices are independent from fault resistance, their values do not deviate from those calculated for bolted faults up to faults with 50  $\Omega$  resistance. Therefore, the proposed fault type classification and phase selection algorithm is robust and can be implemented as simple threshold based comparison. The method is simple and the underline principle is understandable, when compared with algorithms that use tools such as fuzzy logic or machine learning techniques. The proposed method is rigorously evaluated for different fault locations and fault inception angles. Since it is based on initial current transient, phase selection can be done within in about 1 ms time span. Furthermore, as the proposed method uses only locally measured current transients, need of communication is avoided.

## II. FAULT CREATED WAVES AND IDENTIFICATION OF FAULTY PHASES

In three-phase systems, voltages across the capacitances between lines remain at line voltage while the voltages across the capacitances to ground vary. A fault in a transmission line creates a step change and rapid redistribution of charges

---

Naushath M. Haleem and Athula D. Rajapakse are with the University of Manitoba, Winnipeg, Canada (email:ummausha@myumanitoba.ca; athula.rajapakse@umanitoba.ca).

among the capacitances at the location of fault. For example, consider a fault between two lines, the voltage between them becomes zero or very small at the fault. The step change in the voltage between the faulted lines can be represented as the sum of a negative step and a positive step having equal magnitudes, as depicted in Fig. 1 for a fault between Phases-A and B. These step voltages applied at the fault propagate along the lines towards the terminals.

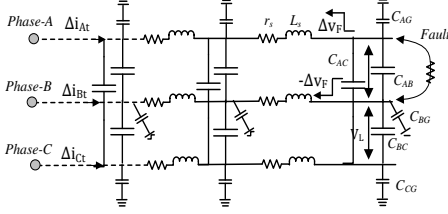


Fig. 1. Fault wave propagation

The changes in terminal currents due to propagated voltage surges can be evaluated by (1).

$$\begin{bmatrix} \Delta i_A(s) \\ \Delta i_B(s) \\ \Delta i_C(s) \end{bmatrix} = \begin{bmatrix} G_{AFk}(s) & G_{BAk}(s) & G_{CAk}(s) \\ G_{ABk}(s) & G_{BFk}(s) & G_{BCK}(s) \\ G_{ACK}(s) & G_{CBk}(s) & G_{CFk}(s) \end{bmatrix} \begin{bmatrix} \Delta V_f(s) \\ -\Delta V_f(s) \\ 0 \end{bmatrix} \quad (1)$$

where  $G_{PFk}(s)$  is the forward transfer function of Phase-P, i.e. change in terminal current in Phase-P due to a change in voltage of Phase-P at the location of fault.  $G_{PQk}(s)$  is the mutual coupling between Phase-P and Phase-Q, i.e. change in terminal current of Phase-Q due to a change in Phase-P voltage at the location of fault. The forward and mutual transfer functions have different frequency characteristics, and the forward transfer function has a greater magnitude than that of the coupling function over certain frequency range (lower frequencies). Within this frequency range, the magnitudes of change in terminal current signals ( $\Delta i_p(s)$ ) of the phases involved in the fault would be larger than the change in the terminal current of the remaining phase. Moreover, the magnitudes of the changes in terminal current signals will be approximately the same for the two phases involved in the fault, due to similar excitation functions ( $\Delta V_f(s)$  and  $-\Delta V_f(s)$ ). For the case shown in Fig. 1,  $|\Delta i_A(s)|$  and  $|\Delta i_B(s)|$  will be larger than  $|\Delta i_C(s)|$  and  $|\Delta i_A(s)| \approx |\Delta i_B(s)|$  within the particular frequency band.

During a line-to-ground fault, the step change in voltage happens in only one phase. According to (2), which considers a Phase-A-to-ground fault, the expected change in current through two remaining phases (Phases-B and C) are govern by the coupling terms.

$$\begin{bmatrix} \Delta i_A(s) \\ \Delta i_B(s) \\ \Delta i_C(s) \end{bmatrix} = \begin{bmatrix} G_{AFk}(s) & G_{BAk}(s) & G_{CAk}(s) \\ G_{ABk}(s) & G_{BFk}(s) & G_{BCK}(s) \\ G_{ACK}(s) & G_{CBk}(s) & G_{CFk}(s) \end{bmatrix} \begin{bmatrix} \Delta V_f(s) \\ 0 \\ 0 \end{bmatrix} \quad (2)$$

Therefore, for the frequency band in which the forward transfer function has greater magnitude than the coupling terms in (2), a larger change in current is expected in the faulty phase. Moreover, the changes in terminal currents of the phases not involved in the fault will be similar in magnitude. For the case considered in (2),  $|\Delta i_A(s)|$  will be larger than  $|\Delta i_B(s)|$  and  $|\Delta i_C(s)|$  while  $|\Delta i_B(s)| \approx |\Delta i_C(s)|$ , within the particular frequency band.

The changes in currents through two-phases are comparable in magnitudes for two phases during both line-to-line and line-to-ground faults. However, a line-to-ground fault can be discriminated from a line-to-line fault by considering whether the magnitude of the change of current in the remaining phase is higher or lower, as explained above. Alternatively, a line-to-ground fault can be reliably recognized from the presence of residual ( $3I_0$ ) current. Although a fast faulty phase selection algorithm can be developed considering the comparison of the changes in terminal currents ( $|\Delta i_p(s)|$  values), they depend on three factors: fault inception angle, fault location, and fault resistance. Therefore, intelligence based approach such as [1], [7] are often used. The change in resistance causes the magnitude of the voltage step in (1) and (2) to change. However, as (1) and (2) represents a linear system, all terminal currents change proportionally. Therefore, influence of fault resistance in comparison of current transient can be mitigated by using the index  $F_{pq}$  defined in (3), which express the change of current in Phase-P relative that of Phase-Q.

$$F_{pq}(s) = \frac{\Delta i_p(s)}{-\Delta i_q(s)} \quad (3)$$

As the index defined in (3) is in the frequency domain, it represents a function that varies with the time. In practical implementation, it is convenient to work with time domain signals with proper filtering. The indices defined as in (4) were found to provide the information required for identifying faulted phases.

$$F_{pq} = \frac{\max |d\hat{i}_p(t)/dt|}{\max |-d\hat{i}_q(t)/dt|} \quad (4)$$

In (4),  $\hat{i}_p(t)$  and  $\hat{i}_q(t)$ , are band limited signals obtained from the currents in Phases P and Q respectively. This is to ensure that signals are in the frequency range where magnitudes of forward transfer functions are greater than those of the coupling terms. In order to mitigate the influence of reflected waves on the index, the maximum is calculated within 1 ms window of time after detecting a fault. Three indices ( $F_{ab}$ ,  $F_{bc}$ , and  $F_{ca}$ ) can be computed considering two phases at a time. Fault type and the faulty phases can be identified based on the values of three indices and the presence or absence of residual current. The index in (4) is closer to unity when the fault is between Phase-P and Phase-Q or Phase-R and ground, greater than unity when Phase-P is involved in a fault while Phase-Q is not involved, and less than unity if only Phase-Q is involved in the fault.

### III. PROPOSED METHOD

Three indices and the instantaneous residual current are calculated continuously until detecting a fault. Upon detecting a fault, values of each index are compared after the time window as depicted in Fig. 2.

For a Phase-P-to-Phase-Q fault, the following three criteria should be satisfied.

- Criterion A1: Since the index associated with two faulty phases is close to the unity;

$$(1 - \epsilon_2) \leq F_{PQ} \leq (1 + \epsilon_3)$$

- Criterion A2: Since the index that expresses the  $\max(di/dt)$  of a faulty phase relative to that of the healthy phase is much larger than unity;

$$(1 + \epsilon_4) \leq F_{PR}$$

- Criterion A3: Since the index that expresses the  $\max(di/dt)$  of the healthy phase relative to that of a faulty phase is less than unity;

$$F_{RP} \leq (1 - \epsilon_5)$$

where R is the healthy phase, and  $\epsilon_1 - \epsilon_5$  are positive tolerance settings.

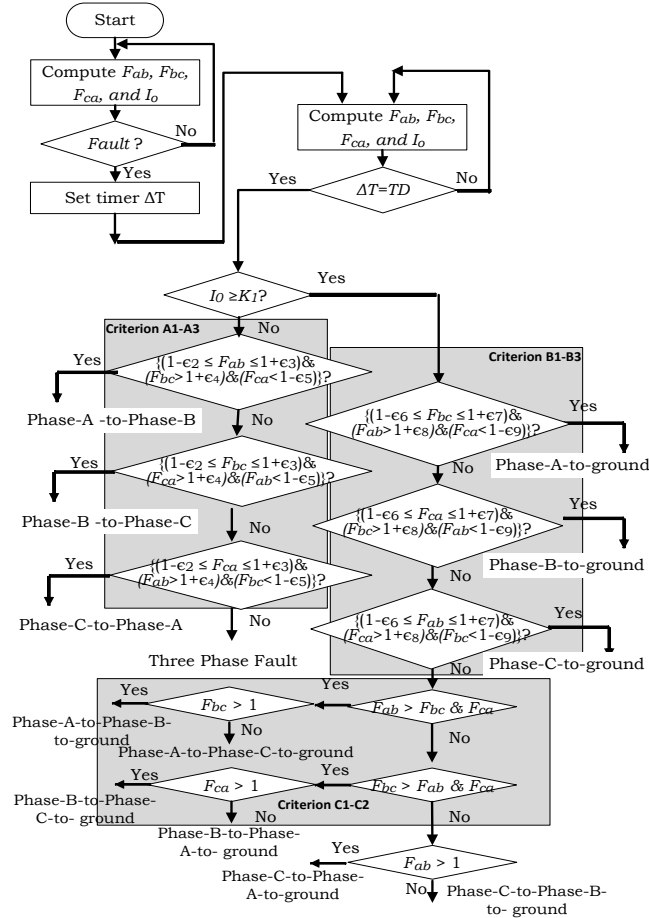


Fig. 2 Proposed fault type and faulty phase (s) identification algorithm

As it will be shown later, three phase faults does not satisfies above three criteria. Upon detecting the presence of instantaneous residual current, the fault is considered as a ground fault and the criteria B1-B3 are tested as depicted in the flowchart of Fig. 2. The criteria for single-phase-to-ground faults, say Phase-P-to-ground fault are given below.

- Criterion B1: Since the index corresponding to the two phases not involved in the fault is close to unity;

$$(1 - \epsilon_6) \leq F_{QR} \leq (1 + \epsilon_7)$$

- Criterion B2: Since the index that expresses the  $\max(di/dt)$  of the faulty phase relative to that of the healthy phase is much larger than unity;

$$(1 + \epsilon_8) \leq F_{PQ}$$

where  $\epsilon_8$  is a positive tolerance setting.

- Criterion B3: Since the index that expresses the

$\max(di/dt)$  of the healthy phase relative to that of a faulty phase is less than unity;

$$F_{RP} \leq (1 - \epsilon_9)$$

where  $\epsilon_6 - \epsilon_9$  are positive tolerance settings.

A line-to-line-to-ground fault is identified by the presence of residual current and failure to satisfy the criteria B1-B3. Upon identifying a line-to-line-to-ground fault, the phase involved in the fault is identified by the index having the greater magnitude. As an example if  $F_{PQ}$  is the largest index, Phase-P is involved in the fault (criterion C1). Then, the index corresponding to two other phases,  $F_{QR}$ , is tested to identify the remaining phase involved in the fault (criterion C2). If  $F_{QR}$  is greater than unity, Phase-Q is involved in the fault; otherwise Phase-R is involved in the fault. Although the outputs of the algorithm are fault types, all information required for faulty phase selection is produced by the algorithm. Fig. 3 shows the proposed method of processing signals and calculating fault type indices. The lower cutoff frequency of the band pass filter is set to avoid the influence of current at power mains frequency and upper cutoff frequency is set to minimize influence of induced transients from other phases in estimating  $\max(di/dt)$  values. As inter conductor capacitance act as high pass filters, induced transients from other phases are more concentrated in the high frequency range. Therefore, band limiting reduces the influence of transient induced from other phases and improves the accuracy of faulty phase(s) identification. The rates of change of currents were computed using the derivative transfer function  $sT$  with a time constant of 0.01s. Process of calculating indices get triggered upon detecting a peak  $di/dt$  greater than a certain threshold level and the maximum values of signal  $di/dt$  are tracked for a period of  $T_D$ .

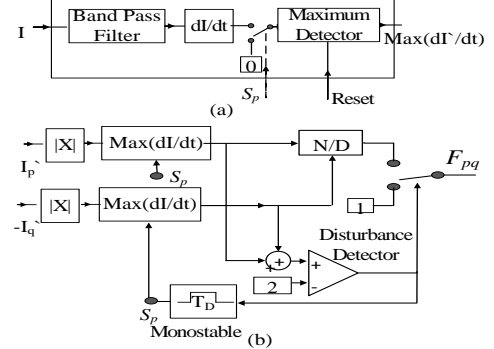


Fig. 3 Signal processing involved in calculating indices (a)  $\text{Max}(di/dt)$  detector, (b) Index estimation

#### IV. TEST SYSTEM

The algorithm is validated using the 230 kV transmission system shown in Fig. 4, simulated in PSCAD electromagnetic transient simulation software.

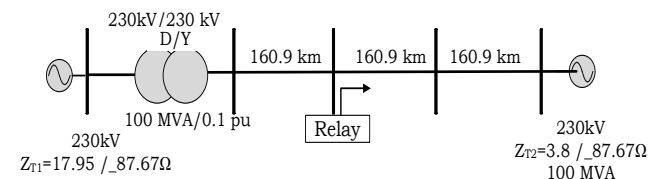


Fig. 4 HV ac test system

Faulty phase detection by the relay protecting middle span of the long transmission line having three sections is presented here, as it is found to be more challenging during the experiments. The transmission line parameters of the test system are given in Table I. Bergeron model of transmission lines are simulated.

TABLE I TRANSMISSION LINE PARAMETERS (@ 60 Hz)

Parameter	Value	Units	Parameter	Value	Units
$R_1$	$5.067 \times 10^{-2}$	$\Omega/\text{km}$	$R_0$	$2.1443 \times 10^{-1}$	$\Omega/\text{km}$
$X_{L1}$	$4.822 \times 10^{-1}$	$\Omega/\text{km}$	$X_{L0}$	1.52566	$\Omega/\text{km}$
$X_{C1}$	0.2947	$\Omega/\text{km}$	$X_{C0}$	0.4144	$\Omega/\text{km}$

The pickup value of the residual current detector is set to 200 A. The lower cut-off frequency of the band pass filter in Fig. 3 is set to 500 Hz. With the help of observed simulation results, upper cut-off frequency is set to 1000 Hz and  $T_D$  is set to 1ms. The simulation time step used (25  $\mu\text{s}$ ) was twenty times smaller than the half period of the highest frequency of the interest, 1000Hz. Finding values for the threshold constants,  $\varepsilon_2$ - $\varepsilon_9$ , is demonstrated in Sections V-B and V-C.

## V. RESULTS

### A. Demonstration of the Basic Algorithm

Fig. 5(a)-Fig. 5(c) shows the voltages, currents, and estimated rate of change of current (ROCO) or ( $di/dt$ ) values respectively for a fault between Phase-A and Phase-B. As per Fig. 5(c), ROCOC values (of the band pass filtered signals) of Phase-A and Phase-B are comparable in magnitude as explained in Section II and Section III. Fulfilment of criteria A1-A3 for a line-to-line fault is shown in Figs. 5(d)–5(f).

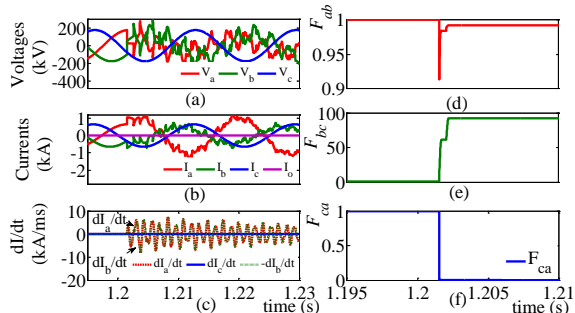


Fig. 5 Responses for Phase-A-to-Phase-B fault at 95 % of the length from the relay (a) Phase voltages, (b) Phase currents, (c) ROCOC values, (d)  $F_{ab}$ , (e)  $F_{bc}$ , (f)  $F_{ca}$

Fig. 6 shows the responses for a Phase-B-to-ground fault. Presence of residual current can be observed in Fig. 6(b).

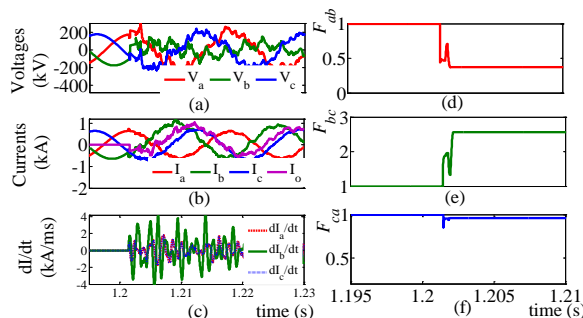


Fig. 6 Responses for a Phase-B-to-ground fault at 75 % away from the relay (a) Phase voltages, (b) Phase currents, (c) ROCOC values, (d)  $F_{ab}$ , (e)  $F_{bc}$ , (f)  $F_{ca}$

The disturbance detector triggers the algorithm about 100  $\mu\text{s}$  after the arrival of fault generated current wave at the terminal. The peak  $di/dt$  values used for computing the indices are frozen 1 ms after the detection of disturbance. Short transient period of indices can be clearly seen from Figs. 6(d)–6(f). Fig. 6(c) shows that the  $di/dt$  values of Phases-A and -C are almost equal, which can also be confirmed from Fig. 6(f) that shows  $F_{ca}$ . Fulfilment of the criteria B2 and B3 can be observed from Figs. 6(d) and 6(f). Having demonstrated the basic waveforms and the fulfillment of criteria for two basic types of faults, influence of the fault inception angle, fault location, and the fault resistance on the estimated indices is rigorously evaluated for each fault type in the next sections.

### B. Identification Faulty Phases for Line-to-Line Faults

Fig. 7 shows the influence of the fault inception angle and the fault resistance for a fault between Phase-A and Phase-B. Indices are estimated for fault resistances 0.05 $\Omega$ , 5 $\Omega$ , and 50 $\Omega$ . The fault inception angle is varied from 0 $^\circ$  to 180 $^\circ$  in 18 $^\circ$  steps. According to Fig. 7, estimated indices do not vary with fault resistance. Indices associated with the healthy phase, Phase-C, significantly change with fault inception angle. The minimum value of the  $F_{bc}$  is 9.56 and the maximum value of  $F_{ca}$  is about 0.01. Therefore, all three criteria, A1-A3, for a line-to-line fault are satisfied for the simulated 33 fault scenarios.

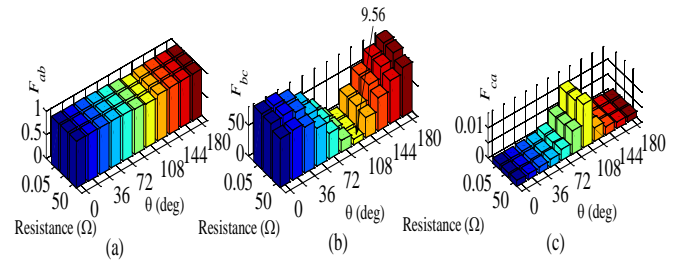


Fig. 7 Indices for Phase A-to-Phase-B faults at 30% under different fault resistances and fault inception angles (a)  $F_{ab}$ , (b)  $F_{bc}$ , (c)  $F_{ca}$

Influence of fault location is evaluated by applying faults between 10% of the line length to 100% in steps of 10%. Fig. 8 depicts estimated indices for Phase-A-to-Phase-C faults at 11 different fault inception angles.

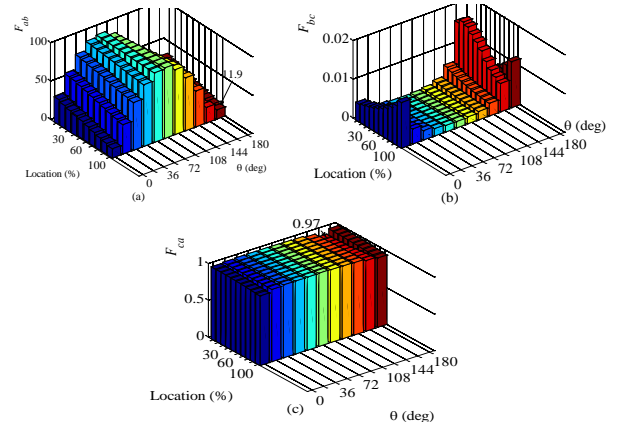


Fig. 8 Fault indices for a solid Phase-A-to-Phase-C faults along the line simulated for every 10% (a)  $F_{ab}$ , (b)  $F_{bc}$ , (c)  $F_{ca}$

According to Figs. 8(a) and 8(b), the worst values of indices

associated with the healthy phase occur for the far end faults. Since the values of indices are significantly dependent on the fault inception angle, indices are estimated for fine intervals of fault inception angles (every  $0.9^\circ$ ) for a far end fault. Fig. 9 shows variation of indices with the fault inception angle. By considering Fig 8(c) and Fig 9(b),  $\varepsilon_3$  can be set to 0 and  $\varepsilon_2$  can be set slightly higher than 0.1. By considering maximum values of the indices corresponding to the healthy phase to the faulty phase shown in Fig. 8(b) and Fig. 9(a),  $\varepsilon_5$  can be set to 0.98. By considering the minimum values of indices corresponding faulty phase to healthy phase shown in Fig. 8(a) and Fig. 9(c),  $\varepsilon_4$  can be set slightly below 6.7. Based on the results for line-to-line faults, it can be concluded that a set of values can be found for  $\varepsilon_2$ - $\varepsilon_5$  that satisfies criteria A1-A3. Therefore, faulty phases for line-to-line faults can be identified accurately with the proposed method.

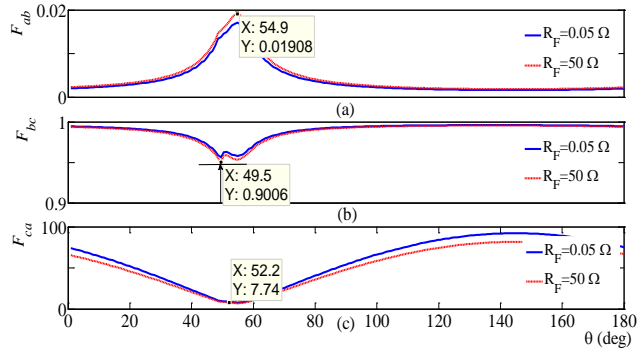


Fig. 9 Fault indices for Phase B-to-Phase-C faults on 95% simulated for every  $0.9^\circ$  deg (a)  $F_{ab}$ , (b)  $F_{bc}$ , (c)  $F_{ca}$

### C. Identification of Faulty Phase for Line-to-Ground Faults

Fig. 10 shows the estimated indices for Phase-A-to-ground fault, for different combinations of fault resistances and fault inception angles. Fig. 11 shows the variation of estimated indices with the fault location for Phase-C-to-ground faults. Fig. 10 is further elaborating the independence of indices from the fault resistance, even when the fault is involving ground currents. It can be seen by Fig. 11 and Fig. 12 that changes in indices with the fault inception angles is less for line-to-ground faults, when compared with the line-to-line faults (see Figs 7 and 8). Therefore, finding threshold constants,  $\varepsilon_6$ - $\varepsilon_9$ , is easier for line-to-ground faults. Considering the range of the values for the index corresponding to the two unfaultry phases, see Fig 11(a) and Fig 12(c),  $\varepsilon_7$  can be set to 0 and  $\varepsilon_6$  can be set slightly larger than 0.347. By considering maximum value of the indices corresponding to healthy phase to faulty phase, see Fig. 11(b) and Fig. 12(a),  $\varepsilon_9$  can be set to slightly lower than 0.46.

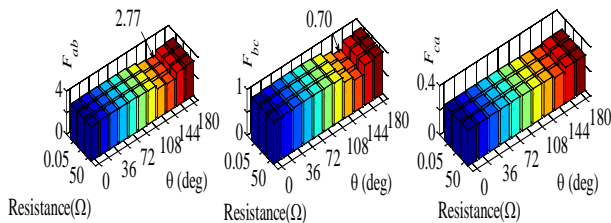


Fig. 10 Fault indices for Phase-A-to-ground faults at 60% (a)  $F_{ab}$ , (b)  $F_{bc}$ , (c)  $F_{ca}$

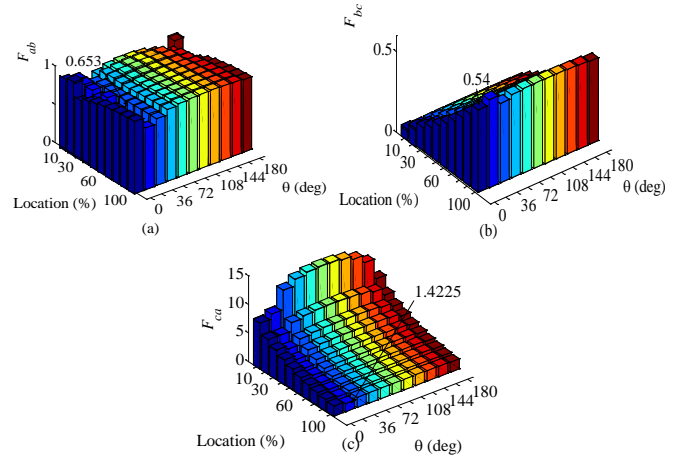


Fig. 11 Fault indices for solid Phase-C-to-ground faults along the line (a)  $F_{ab}$ , (b)  $F_{bc}$ , (c)  $F_{ca}$

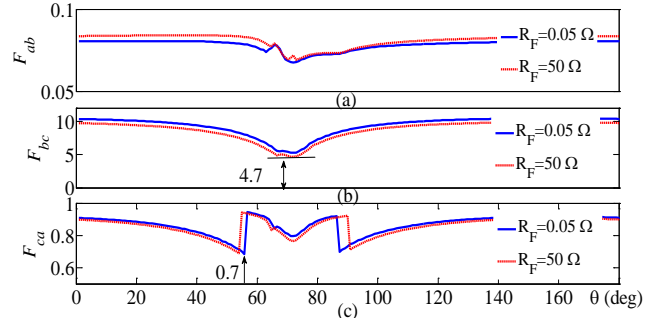


Fig. 12 Indices for Phase-B-to-ground faults at 85% (a)  $F_{ab}$ , (b)  $F_{bc}$ , (c)  $F_{ca}$

Considering the minimum values of indices corresponding to faulty phase to healthy phase  $di/dt$  values, see Fig. 11(c) and Fig 12(b),  $\varepsilon_8$  can be set slightly lower than 0.42. As the line-to-ground fault is the most common type fault in transmission line, ability to accurately identify faulty phase raise overall accuracy significantly.

### D. Discriminating Three Phase Faults from Line-to-Line Faults

Figs. 13(a)-13(c) prove that the fault resistance does significantly affect the algorithm, even during three phase faults. According to Fig. 2, three phase faults are discriminated from line-to-line faults by the absence of residual current component and failure to fulfill criteria A1 to A3. This is proved with the help of estimated fault indices for a close-up and remote faults for different fault inception angles (varied in small steps) shown in Fig 13(d)-13(f).

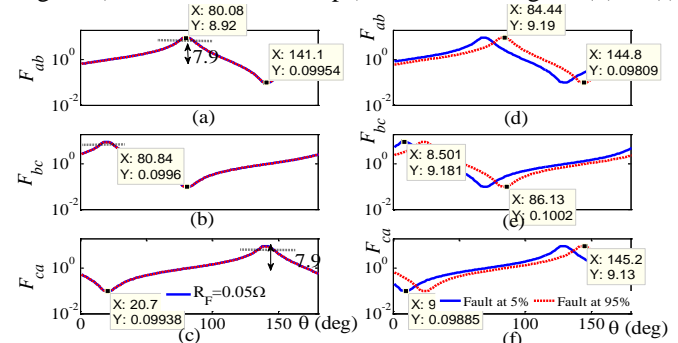


Fig. 13 (a)-(c) Indices for solid and  $50 \Omega$  3-phase faults at 50%, (d)-(f) Indices for solid faults at 5% and 95% of the line

As per Fig. 13(d)-13(f) showing estimated indices for faults at 5% and 95 % away from the relay, only for a very short span of angle criterion A2 is valid. However, the criterion A3 is invalid for all fault scenarios as minimum value of indices, 0.09, is higher than  $1 - \epsilon_5$ , 0.02. Therefore, it can be concluded that any three phase fault doesn't satisfies the criteria A1-A3 simultaneously.

### E. Identification Faulty Phases for Line-to-Line-to-ground Faults

Fig. 14(a) shows the indices for Phase-A-to-Phase-B-to-ground fault at 45% of the line length. Phase-B is involved in the fault for fault inception angle  $54^\circ$  as per criterion C1 since value of  $F_{bc}$  is the greatest among three indices. As the index associated with two remaining phases,  $F_{ca}$ , is less than unity (see Table-II showing the numerical values), Phase-A can be identified as involved in the fault as per criterion C2. Furthermore, as per Fig. 14(b), indices do not significantly vary with the fault resistance even for the line-to-line-to-ground faults. Fulfillment of criteria C1 and C2 for line-to-line-to-ground fault can be verified with Table-II which shows indices for Phase-A-to-Phase-B-to-ground faults at 45% of the line (Scenario-1), and Phase-A-to-Phase-C-to-ground faults at 60% of the line (Scenario-2) for some angles.

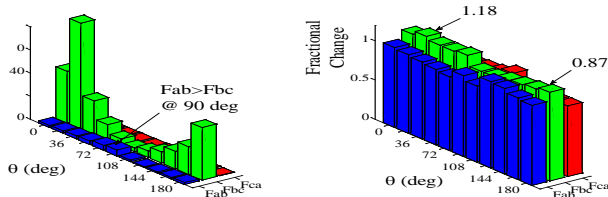


Fig. 14 Fault indices for Phase-A-to-Phase-B-to-ground faults at 45% (a) Indices for a  $0.05 \Omega$  faults, (b) Per unit change in indices for  $50\Omega$  faults

TABLE II  
FAULTY PHASE IDENTIFICATION USING CRITERIA C1 AND C2

Scenario	Angle	$F_{ab}$	$F_{bc}$	$F_{ca}$	Crit.C1	Crit.C2
1	$54^\circ$	1.491	6.677	0.088	B	A
1	$90^\circ$	2.540	1.455	0.238	A	B
1	$162^\circ$	0.659	11.915	0.111	B	A
2	$54^\circ$	11.676	0.096	0.755	A	C
2	$126^\circ$	3.161	0.168	1.679	A	C

Possibility of misclassifying line-to-line-to-ground faults is evaluated by simulating faults in small intervals of fault inception angles. As per Fig. 15, criterion C1 identifies one phase involved in the fault, Phase-B or Phase-C, accurately from  $0^\circ$  to  $180^\circ$ . However, for  $10^\circ$  span between Point-A1 and Point-A2, criterion C2 declares as Phase-A is involved in the fault rather than Phase-B as  $F_{ab} > 1$ .

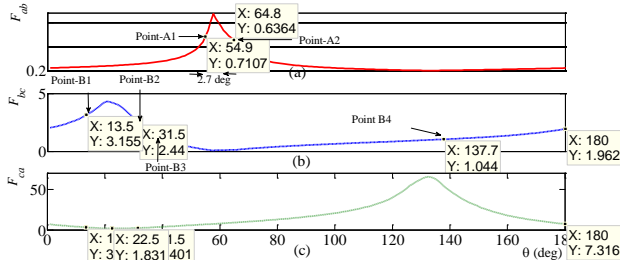


Fig. 15 Fault indices for Phase-B-to-Phase-C-to-ground faults at 45% at every 0.9 deg (a)  $F_{ab}$ , (b)  $F_{bc}$ , (c)  $F_{ca}$

Possibility of misclassifying line-to-line-to-ground faults as a line-to-ground fault is analyzed by testing criteria B2 and B3 for intervals where one index is close to unity,  $10^\circ$  span between point-A1 and Point-A2. However, around span between Point-A1 and Point-A2, it can be classified as a Phase-C-to-ground fault as both criteria B2 and B3 are satisfied. Therefore, if a line-line-to-ground fault happens within about  $5^\circ$  around the zero crossing of one phase, the method could erroneously declare a single phase to ground fault.

## VI. CONCLUSIONS

A novel fast fault type and faulty phase detection algorithm based on incremental current signals was proposed. The results of rigorous evaluation show that the indices proposed in this paper are very effective for simplifying the faulty phase identification problem. The effect of fault resistance on the proposed fault indices is minimal and a set of threshold values can be found easily for comparison used in the faulty phase selection algorithm. Simplicity of the method facilitates for easy implementation with low cost hardware and avoids the need for generating large training data sets. Currently, the application of the method is restricted to grounded systems. Further research is being conducted to understand practical aspects such as impacts of signal noise, threshold settings, delays in the triggering mechanisms, and extension to delta connected systems.

## VII. REFERENCES

- [1] N. Perera and A. D. Rajapakse, "Recognition of Fault Transients Using a Probabilistic Neural-Network Classifier," in *IEEE Trans. on Power Del.*, vol. 26, no. 1, pp. 410-419, Jan. 2011.
- [2] K. M. Silva, B. A. Souza and N. S. D. Brito, "Fault detection and classification in transmission lines based on wavelet transform and ANN," in *IEEE Trans. on Power Del.*, vol. 21, no. 4, pp. 2058-2063, Oct. 2006.
- [3] Su Qianli, Dong Xinzhou, Z. Q. Bo and F. Jiang, "New approach of fault detection and fault phase selection based on initial current traveling waves," *IEEE Power Engineering Society Summer Meeting*, Chicago, IL, USA, pp. 393-397, Jul. 2002.
- [4] Z. He, L. Fu, S. Lin and Z. Bo, "Fault Detection and Classification in EHV Transmission Line Based on Wavelet Singular Entropy," in *IEEE Trans. on Power Del.*, vol. 25, no. 4, pp. 2156-2163, Oct. 2010.
- [5] F. B. Costa, B. A. Souza and N. S. D. Brito, "Effects of the fault inception angle in fault-induced transients," in *IET Generation, Transmission & Distribution*, vol. 6, no. 5, pp. 463-471, May 2012.
- [6] X. Dong, J. Wang, S. Shi, B. Wang, B. Dominik and M. Redefern, "Traveling wave based single-phase-to-ground protection method for power distribution system," in *CSEE Journal of Power and Energy Systems*, vol. 1, no. 2, pp. 75-82, June 2015.
- [7] M. Ben Hessine, S. Marrouchi and S. Chebbi, "A fault classification scheme with high robustness for transmission lines using fuzzy-logic system," *2017 International Conference on Advanced Systems and Electric Technologies (IC\_ASET)*, Hammamet, Tunisia, pp. 256-261, Jan. 2017.
- [8] F. B. Costa, A. Monti, F. V. Lopes, K. M. Silva, P. Jamborsalamati and A. Sadu, "Two-Terminal Traveling-Wave-Based Transmission-Line Protection," in *IEEE Transactions on Power Delivery*, vol. 32, no. 3, pp. 1382-1393, June 2017.
- [9] L. Shang, G. Herold and J. Jaeger, "A new approach to high-speed protection for transmission line based on transient signal analysis using wavelets," *2001 Seventh International Conference on Developments in Power System Protection (IEE)*, Amsterdam, Netherlands, pp. 173-176, Apr. 2001.